Use of transpiration for reduction of resistance to relative movement of parallel plates

Longyin Jiao [1,*] and J. M. Floryan [2,†]
[1] School of Aerospace Engineering, Beijing Institute of Technology, Beijing 100081, People's Republic of China
[2] Department of Mechanical and Materials Engineering, The University of Western Ontario, London, Ontario, Canada N6A 5B9

(Received 5 July 2020; accepted 26 October 2020; published 11 January 2021)

An analysis of the effects of transpiration on the forces required to maintain the relative movement of parallel plates has been carried out using a two-dimensional model problem. Transpiration was placed either at the stationary or at the moving plates. In both cases its spatial distribution was made of periodic components, but the explicit results are provided only for the commensurable systems. It is shown that the force required to maintain plate movement is affected by the reduction of the effective spacing between the plates caused by formation of a cushion made of the transpiration "bubbles," by the elimination of the direct contact between the fluid in the slot and the plate with transpiration, and by nonlinear streaming generated by the transpiration. It is possible to reduce the pulling force through the proper selection of the transpiration pattern. The transpiration wave number resulting in the largest reduction corresponds to the maximization of the nonlinear streaming. The largest reduction of resistance is achieved by concentrating transpiration at a single transpiration wave number and avoiding commensurability effects. An analysis of finite-slot transpiration demonstrates the existence of the reduced distribution model, i.e., the performance of such systems can be well approximated using just a few leading modes from the Fourier expansions describing such transpirations. The analysis of energy costs shows that the overall energy cost of the modified flow is higher than the cost of the unmodified flow. Conditions leading to the minimization of this cost have been identified. These conditions describe the most effective use of transpiration as a propulsion augmentation system. Transfer of transpiration to the moving plate does not affect the reduction of resistance and does not change the energy cost associated with transpiration.

DOI: 10.1103/PhysRevFluids.6.014101

I. INTRODUCTION

The performance of numerous machines is affected by friction between moving parts as it affects both the energy cost as well as wear [1]. This cost may be estimated by determining the force required to maintain the relative movement of these parts. Similar motions can be found in other applications, e.g., the towing of a free-floating body in a shallow basin. In all cases the reference model is that of a flow which forms in a slot formed by two infinite parallel plates in relative motion, i.e., Couette flow. This flow is characterized by the absence of a streamwise pressure gradient, a linear velocity distribution across the fluid layer and the lack of the linear stability limit [2]. The nonlinear stability analyses are well reviewed in Ref. [3] and demonstrate various routes to

*Visiting graduate student.
†floryan@uwo.ca

secondary finite-amplitude states as well as to turbulence. Surface modifications either in the form of transverse grooves [4], axisymmetric ribs [5] or wall transpiration [6] can lead to centrifugal instabilities. Replacing the plane Couette flow with the annular Couette flow leads to additional shear instabilities [7]. Transition to secondary states leads to an increase in the plate shear and the need to increase the external driving force. Such states should be avoided if minimization of the energy cost is of interest.

The present work is part of a wider search for drag reducing methods whose effectiveness is, in the present case, measured by the reduction of the external force required to maintain the relative plate movement. One way to approach this problem is to assure stability of the flow so that transition to secondary states is avoided. Here we follow a different approach: we look for spatial modulations which could lead to the reduction of shear. This approach is preferable for the highly stable low Reynolds number laminar flows. The use of grooves for this purpose has been explored in Refs. [8,9] while modulations created by spatially distributed heating and their effect on drag reduction have been discussed in Ref. [10]. The focus of the present work is on the use of wall transpiration, whose studies go back to Ref. [11], where transpiration was used to mimic surface roughness and to determine its effect on the laminar-turbulent transition. The same concept was used in the analysis of channel flow [12] and boundary layers [13–15]. Direct numerical simulations showed that transpiration can initiate a bypass route to the laminar-turbulent transition [16]. Alternative drag reducing techniques involve more sophisticated modifications of surface topography [17], plasma- [18], sound- [19], and piezo-driven [20] actuators as well as surface vibrations [21], whose use is yet to be explored in Couette flow.

Wall transpiration found applications in cooling of surfaces exposed to high temperature fluids [22–24]. Maintaining a stable layer of injected low temperature fluid is the primary goal as this layer prevents a direct contact between the high temperature fluid and the solid wall. The possible reduction of wall shear associated with this technique is yet to be explored. A completely different concept involves injection of cold fluid and extraction of an equal mass of hot fluid as this provides a means for extracting heat flux from the conduit. The possible reduction of shear is yet to be explored in the context of this application.

Wall transpiration can be viewed as an active flow control method, which implies the use of external energy. It has been shown that in the case of pressure driven flows the laminar unmodulated state represents the lowest energy state [25]. This proof has been extended to Couette flow [26]. While the energy savings associated with the reduction of resistance may not surpass the energy expenditures implied by the flow control process, one can look at it as a part of the overall propulsion system where one can expend energy on reducing resistance rather than increasing the propulsive force so that the existing system can deliver an improved performance. If the maximum possible propulsive force has been achieved, then the only way to increase the system performance is to expend energy on resistance reduction. An additional benefit is due to the decrease of the wall shear stress which reduces the long-term wear of surfaces exposed to such shear. Similar effects are known to occur in pressure-gradient-driven turbulent flows [27–29].

The presentation is organized as follows. Section II presents a two-dimensional model problem involving two parallel plates with the lower plate being equipped with a transpiration system. Section III describes the method of solution. Section IV describes the performance and possible resistance reduction in a system utilizing unimodal transpiration. Section IVA discusses transpiration-induced changes in the external force required to maintain the movement of the upper plate. Section IVB describes nonlinear streaming and self-propulsion generated by this effect. Section IVC provides a description of the properties of the modulated flow. Section IVD discusses energy requirements associated with transpiration. Section V describes multimodal transpiration and commensurability effects. Section VI discusses the use of finite-size transpiration slots and their effectiveness. Section VII discusses changes in the system performance when the transpiration is applied at the moving plate. Section VIII provides a short summary of the main conclusions.

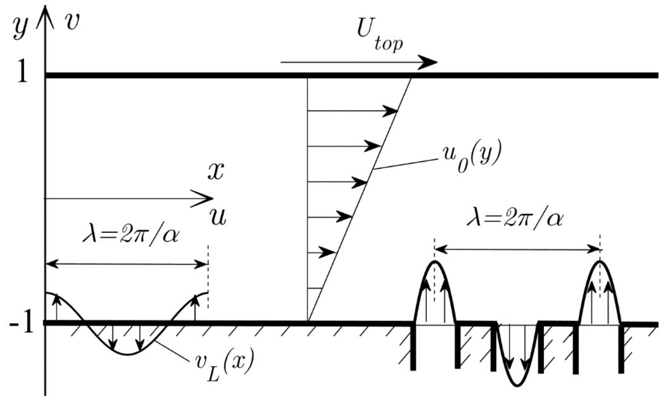

FIG. 1. Sketch of the flow configuration. Left side, continuous transpiration; right side, transpiration through discrete slots.

II. PROBLEM FORMULATION

Consider two horizontal plates moving relative to each other and separated by a distance $2h$. The resulting gap extends to $\pm\infty$ in the x direction and is filled with a fluid of kinematic viscosity ν, dynamic viscosity μ and density ρ. The upper plate is pulled in the positive x direction with a constant velocity U_{top} with its movement resisted by viscous friction, while the lower plate is stationary. The velocity and pressure fields, the pulling force, the shear acting on the upper plate and the flow rate generated by moving plate have the form

$$\boldsymbol{v}_0(x, y) = [u_0, v_0] = \left[\frac{(1+y)}{2}, 0\right], \quad p_0(x, y) = C, \quad F_0 = \frac{1}{2}, \quad \tau_0 = -\frac{1}{2}, \quad Q_0 = 1, \tag{2.1}$$

where h has been used as the length scale, $\boldsymbol{v}_0$ stands for the velocity vector scaled with U_{top} as the velocity scale with $[u_0, 0]$ components in the $[x,y]$ directions, p_0 denotes the pressure scaled with ρU_{top}^2 as the pressure scale, F_0 denotes the force per unit length and width required to pull the upper plate scaled with $U_{\text{top}}\mu/h$, τ_0 stands for the shear acting on the upper plate scaled with $U_{\text{top}}\mu/h$, Q_0 stands for the flow rate scaled with the same velocity scale and the relevant Reynolds number is defined as $\text{Re} = U_{\text{top}}h/\nu$. The above flow represents the reference state and all relevant quantities have been identified using subscript 0.

To change the pulling force, we introduce a spatially distributed transpiration at the lower plate (see Fig. 1) and represent the resulting flow as a superposition of the unmodified flow and the transpiration-driven modifications. The complete flow quantities have the form

$$\begin{gathered}\boldsymbol{v}_c(x, y) = [u_c(x, y), v_c(x, y)] = [\text{Re}\, u_0(y) + u_1(x, y), v_1(x, y)], \qquad p_c(x, y) = p_1(x, y) + \text{const}, \\ Q_c = \text{Re}\, Q_0 + Q_1, \quad \tau_c = \text{Re}\, \tau_0 + \tau_1, \quad F_c = \text{Re}\, F_0 + F_1,\end{gathered} \tag{2.2}$$

where $[u_c, v_c]$ and $[u_1, v_1]$ stand for the $[x,y]$ components of the complete velocity vector and the velocity vector modifications, respectively, p_c, Q_c, F_c stand the complete pressure, the flow rate and the puling force, respectively, and p_1, Q_1 and F_1 denote the velocity, the pressure, the flow rate and the pulling force modifications, respectively. The complete flow quantities and the modifications have been scaled with the viscous velocity scale $U_v = \nu/h$ where $U_{\text{top}}/U_v = Re$, the complete pressure field and the pressure modifications have been scaled using ρU_v^2 as the pressure scale, the complete shear and shear modifications as well as the complete force and force modifications have been scaled with $U_v\mu/h$.

Transpiration may have an arbitrary pattern but cannot carry any net mass flux. We shall represent it using a Fourier expansion of the form

$$u_1(x,-1)=0, \quad v_1(x,-1)=\mathrm{Re}_T \sum_{n=-N_L, n\neq 0}^{n=+N_L} s_T^{(n)} e^{in\alpha x}, \tag{2.3a}$$

$$u_1(x,+1)=0, \quad v_1(x,+1)=0, \tag{2.3b}$$

where $\mathrm{Re}_T = V_T h/\nu$ is the transpiration Reynolds number, V_T is the difference between the maximum and minimum of v_1, i.e.,

$$V_T = \max(v_1) - \min(v_1), \tag{2.3c}$$

$s_T^{(n)}$'s have been scaled with V_T so that

$$-\frac{1}{2} \leqslant \sum_{n=-N_G}^{n=N_G} s_T^{(n)} e^{in\alpha x} \leqslant \frac{1}{2}, \tag{2.3d}$$

the reality conditions require that $s_T^{(n)} = s_T^{(-n)^*}$ where stars denote complex conjugates, α is the transpiration wave number and $\lambda = 2\pi/\alpha$ is its wavelength, and N_T denotes the number of Fourier modes required to describe the transpiration distribution.

The pulling force can be determined by solving the field equations of the form

$$\frac{\partial u_1}{\partial x} + \frac{\partial v_1}{\partial y} = 0, \tag{2.4a}$$

$$(\mathrm{Re}\, u_0 + u_1)\frac{\partial u_1}{\partial x} + \mathrm{Re}\, v_1 \frac{du_0}{dy} + v_1 \frac{\partial u_1}{\partial y} = -\frac{\partial p_1}{\partial x} + \nabla^2 u_1, \tag{2.4b}$$

$$(\mathrm{Re}\, u_0 + u_1)\frac{\partial v_1}{\partial x} + v_1 \frac{\partial v_1}{\partial y} = -\frac{\partial p_1}{\partial y} + \nabla^2 v_1, \tag{2.4c}$$

where ∇^2 denotes the Laplace operator. Since introducing transpiration cannot create a mean streamwise pressure gradient, one needs to impose the pressure gradient constraint of the form

$$\left.\frac{\partial p_1}{\partial x}\right|_{\mathrm{mean}} = 0. \tag{2.5}$$

The question of the determination of changes of the pulling force is posed as the question of finding the additional force which needs to be applied at the upper plate to maintain the same velocity with transpiration as without transpiration.

The pulling force must overcome viscous friction. The change of this force per unit length and width of the plate can be expressed as

$$F_1 = F_c - \mathrm{Re}\, F_0 = \lambda^{-1} \int_0^{\lambda} \left.\frac{\partial u_1}{\partial y}\right|_{y=1} dx. \tag{2.6}$$

Negative F_1 corresponds to a reduction of resistance and $F_c = 0$ identifies conditions when the pulling force is reduced to zero. Negative F_c indicates a need to reverse the direction of this force, i.e., the pulling forces needs to be replaced by a braking force to maintain the prescribed plate velocity. Another measure of resistance is the change Q_1 in the fluid volume being pulled by the plate

$$Q_1 = Q_T - \mathrm{Re}\, Q_0 = \left.\left(\int_{-1}^{1} u_1(x,y)dy\right)\right|_{\mathrm{mean}}, \tag{2.7}$$

with positive Q_1 corresponding to an increase of the flow rate and reduction of resistance.

III. METHOD OF SOLUTION

The solution method is explained in detail in Ref. [30] and, thus, the following presentation is limited to a short outline. We define the stream function $\psi(x, y)$ in the usual manner, i.e., $u_1 = \partial\psi/\partial y$, $v_1 = -\partial\psi/\partial x$, and eliminate pressure bringing the governing equations to the following form:

$$\nabla^4\psi - \text{Re}\, u_0 \frac{\partial}{\partial x}(\nabla^2\psi) + \text{Re}\frac{d^2 u_0}{dy^2}\frac{\partial\psi}{\partial x} = NN(x, y), \tag{3.1a}$$

where the nonlinear term NN is expressed as

$$NN(x, y) = \frac{\partial}{\partial y}\left(\frac{\partial\langle u_1 u_1\rangle}{\partial x} + \frac{\partial\langle u_1 v_1\rangle}{\partial y}\right) - \frac{\partial}{\partial x}\left(\frac{\partial\langle u_1 v_1\rangle}{\partial x} + \frac{\partial\langle v_1 v_1\rangle}{\partial y}\right), \tag{3.1b}$$

∇^4 denotes the biharmonic operator and $\langle f\, g\rangle$ denotes product of functions f and g. The solution is assumed to be in the form of Fourier expansions, i.e.,

$$(x, y) = \sum_{n=-\infty}^{n=+\infty} \varphi^{(n)}(y)e^{in\alpha x}, \quad u_1(x, y) = \sum_{n=-\infty}^{n=+\infty} u_1^{(n)}(y)e^{in\alpha x},$$

$$v_1(x, y) = \sum_{n=-\infty}^{n=+\infty} v_1^{(n)}(y)e^{in\alpha x}, \quad p_1(x, y) = \sum_{n=-\infty}^{n=+\infty} p_1^{(n)}(y)e^{in\alpha x}, \tag{3.2}$$

where $u_1^{(n)} = D\varphi^{(n)}$, $v_1^{(n)} = -in\alpha\varphi^{(n)}$, $\varphi^{(n)} = \varphi^{(-n)*}$, ${u_1}^{(n)} = {u_1}^{(-n)*}$, ${v_1}^{(n)} = {v_1}^{(-n)*}$, ${p_1}^{(n)} = {p_1}^{(-n)*}$, $D = d/dy$, and stars denote complex conjugates. In addition, Fourier expansions representing various products as well as nonlinear terms are represented in the following forms:

$$[\langle u_1 u_1\rangle, \langle u_1 v_1\rangle, \langle v_1 v_1\rangle, NN\,] = \sum_{n=-\infty}^{n=+\infty}[\langle u_1 u_1\rangle^{(n)}, \langle u_1 v_1\rangle^{(n)}, \langle v_1 v_1\rangle^{(n)}, NN^{(n)}](y)e^{in\alpha x}. \tag{3.3}$$

Substitution of Eq. (3.2) into Eq. (3.1) and separation of Fourier components result in a system of ordinary differential equations for the modal functions of the form

$$D_n^2\varphi^{(n)} - in\alpha\text{Re}(u_0 D_n - D^2 u_0)\varphi^{(n)} = NN^{(n)}, \tag{3.4}$$

where $D^2 = d^2/dy^2$, $D_n = D^2 - n^2\alpha^2$, $NN^{(n)} = in\alpha D\langle u_1 u_1\rangle^{(n)} + D^2\langle u_1 v_1\rangle^{(n)} + n^2\alpha^2\langle u_1 v_1\rangle^{(n)} - in\alpha D\langle v_1 v_1\rangle^{(n)}$, $-\infty < n < +\infty$. The boundary conditions for the modal functions are expressed as

$$\varphi^{(0)}(-1) = 0, \tag{3.5a}$$

$$\varphi^{(n)}(-1) = i\text{Re}_T s_T^{(n)}/n\alpha \quad \text{for } 1 \leqslant n \leqslant N_L, \quad \varphi^{(n)}(-1) = 0 \quad \text{for } n > N_L, \tag{3.5b}$$

$$\varphi^{(n)}(+1) = 0 \quad \text{for} \quad -\infty < n < -1, \quad 1 < n < +\infty, \tag{3.5c}$$

$$D\varphi^{(n)}(-1) = 0 \quad \text{for} \quad -\infty < n < +\infty, \tag{3.5d}$$

$$D\varphi^{(n)}(+1) = 0 \quad \text{for} \quad -\infty < n < +\infty. \tag{3.5e}$$

To determine the form of the condition corresponding to the fixed mean pressure gradient constraint, insert Eq. (3.2) into the x-momentum equation and extract the aperiodic term to arrive at

$$D^2\varphi^{(0)}(1) - D^2\varphi^{(0)}(-1) = 0, \tag{3.5f}$$

which is the final boundary condition.

System Eqs. (3.4) and (3.5) are solved numerically using Chebyshev expansions for the modal functions, Galerkin procedure for the conversion of the differential equations into algebraic equations and the *Tau* method for incorporation of the boundary conditions [31].

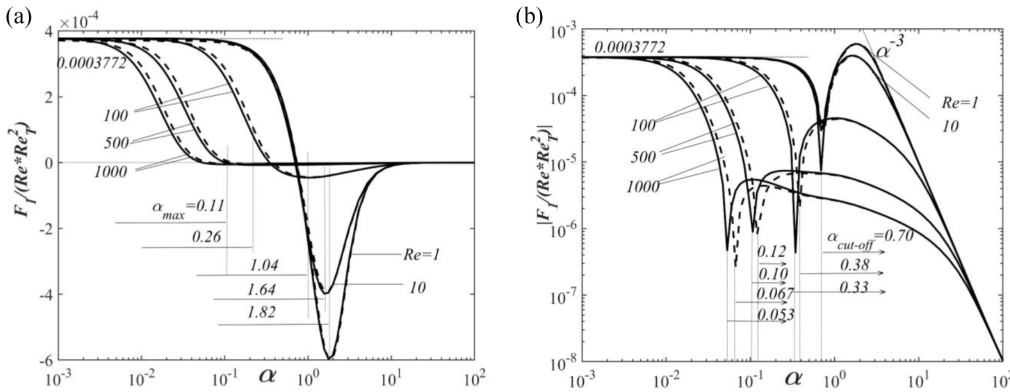

FIG. 2. Change F_1 of the driving force which needs to be applied at the upper plate to maintain its movement for Re = 10, and $\mathrm{Re}_T = 2$ (solid lines) and $\mathrm{Re}_T = 10$ (dashed lines). Variations of F_1 in the limit $\alpha \to \infty$ limit are illustrated in Fig. 2(b). The areas to the right of the cutoff wave numbers α_{cutoff} correspond to a reduction of F_1. The maximum force reductions are achieved at wave numbers $\alpha_{\max}$.

The pressure modal functions are computed by inserting Eq. (3.2) into Eq. (2.4b) and separating Fourier modes resulting in

$$p_1^{(n)} = \frac{-i}{n\alpha}\left[(D^2 - n^2\alpha^2 - in\alpha\,\mathrm{Re}u_0)D\varphi^{(n)} + in\alpha\,\mathrm{Re}\frac{du_0}{dy}\varphi^{(n)} - in\alpha u_1 u_1{}^{(n)} - Du_1 v_1{}^{(n)}\right], \quad n \neq 0. \tag{3.6a}$$

The modal function $p_1^{(0)}$ is computed by inserting Eq. (3.2) into Eq. (2.4c) and extracting the zeroth mode resulting in the following expression:

$$p_1^{(0)} = -\langle v_1 v_1\rangle^{(0)} + \mathrm{const}, \tag{3.6c}$$

where the integration constant is selected by setting the mean part p_{mean} of the pressure to zero, i.e.,

$$p_{\mathrm{mean}} = \frac{1}{2\lambda}\int_{-1}^{1}\int_{0}^{\lambda}\left[\sum_{n=-\infty}^{n=+\infty}(p^{(n)}e^{in\alpha x}) + \mathrm{const}\right]dxdy = \frac{1}{2}\int_{-1}^{1} p^{(0)}dy + \mathrm{const} = 0. \tag{3.6d}$$

IV. UNIMODAL TRANSPIRATION

We shall start the discussion with the simplest transpiration pattern characterized by a single Fourier mode (unimodal transpiration) leading to boundary conditions at the lower plate of the form

$$u_1(x, -1) = 0, \quad v_1(x, -1) = \tfrac{1}{2}\mathrm{Re}_T\cos(\alpha x). \tag{4.1}$$

Changes of the pulling force and the flow rate can be expressed as

$$F_1 = D^2\varphi^{(0)}(1)\,, \quad Q_1 = \varphi^{(0)}(1). \tag{4.2}$$

A. Changes of the flow resistance

A preferable measure of the flow resistance is the change of the pulling force required to maintain movement of the upper plate. Its variations illustrated in Fig. 2 show a rather complex system response. Our interest is in the negative values of F_1 as they correspond to a reduction of resistance. The reduction is possible to achieve but only if the transpiration wave number is larger than a certain cutoff α_{cutoff}. Reduction of α below α_{cutoff} leads to an increase of resistance with the limit of F_1 for $\alpha \to 0$ being proportional to $\mathrm{Re} * \mathrm{Re}_T^2$. Increasing α above α_{cutoff} leads to a reduction of resistance but its excessive increase will reduce this effect proportionally to α^{-3} when $\alpha \to \infty$. Wave numbers leading to the maximum reduction of resistance are identified as $\alpha_{\max}$.

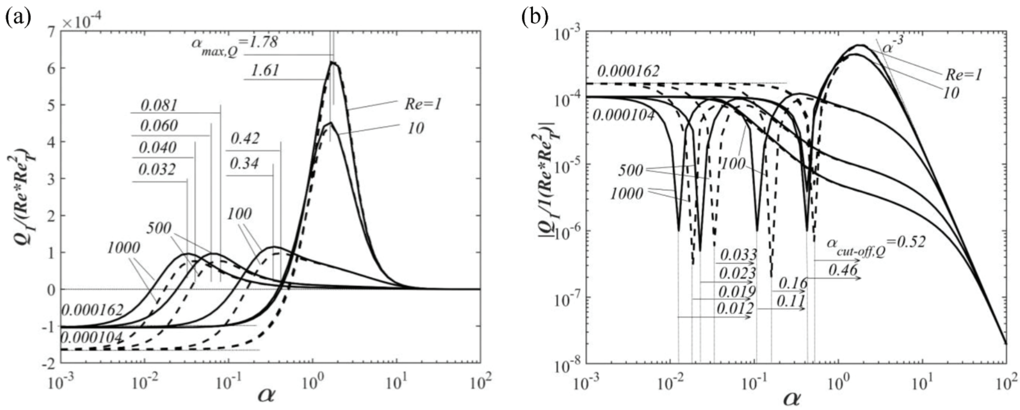

FIG. 3. Change of the flow rate Q_1 caused by transpiration for $\mathrm{Re}_T = 2$ (solid lines) and $\mathrm{Re}_T = 10$ (dashed lines). Variations of Q_1 in the limit $\alpha \to \infty$ are illustrated in Fig. 2(b). The areas to the right of the cutoff wave numbers $\alpha_{\mathrm{cutoff},Q}$ correspond to an increase of Q_1. The maximum flow rate increases are achieved at wave numbers $\alpha_{\mathrm{max},Q}$.

The same effect can be illustrated using the change in the amount of fluid Q_1 being pulled by the plate. Since the transpiration is applied at the stationary plate, the friction there is changed which means that the fluid in the slot will be more affected by the movement of the upper plate, i.e., the flow rate is expected to be reduced when the friction increases and to be increased when the friction decreases. This prediction is confirmed by the results presented in Fig. 3, which show an increase of the flow rate for transpiration wave numbers larger than the cutoff wave number $\alpha_{\mathrm{cutoff},Q}$ but $\alpha_{\mathrm{cutoff},Q}$ are somewhat different from those determined using F_1. Similarly, the maximum increase of the flow rate is achieved at $\alpha_{\mathrm{max},Q}$ which is somewhat different from α_{max}. These differences suggest a delicate balance between different mechanisms contributing to the formation of resistance for conditions where change from the resistance increase to the resistance decrease is observed. We shall use F_1 as the base measure of resistance change for the remainder of this discussion.

Changes of F_1 can be explained by looking at the flow topologies illustrated in Fig. 4 which demonstrate the formation of a "cushion" made of "bubbles" of fluid injected through the plate preventing direct contact between the fluid being dragged by the upper plate and the lower plate. This effect is expected to lead to a reduction of resistance. The finite thickness of this "cushion" reduces the effective spacing between the plates which leads to an increase of shear and, in this sense, increases the movement resistance. The "cushion" thickness strongly depends on the transpiration wave number as it is a function of the fluid volume $Q_T = 2\mathrm{Re}_T/\alpha$ injected into the slot per half wavelength, i.e., it is large for the long-wavelength transpiration and rapidly diminishes for the short-wavelength transpiration. It also depends on the Reynolds number as faster movement of the upper plate limits penetration of the injected fluid into the slot. As a result, spatial flow modulations can be found everywhere in the slot for small α's while these modulations are confined to a thin boundary layer attached to the lower plate for large α's. In this limit, the fluid being pulled by the upper plate lifts above the lower plate and slides on the "cushion" made of the injected fluid. This effect is well illustrated by plots of u_1 at locations corresponding to the maxima of suction and blowing displayed in Fig. 5. Large modulations can be seen everywhere in the slot for small α's while there is a clear distinction between the modulated boundary layer near the lower plate and the unmodulated flow above with a characteristic linear velocity distribution.

Variations of the external force required to maintain the specified velocity of the upper plate as a function of α displayed in Fig. 2 demonstrate an increase of this force for small α's indicating the dominance of effects associated with the reduction of the effective distance between the plates. Large Q_T requires a larger force as the amount of mass which needs to be driven from the injection

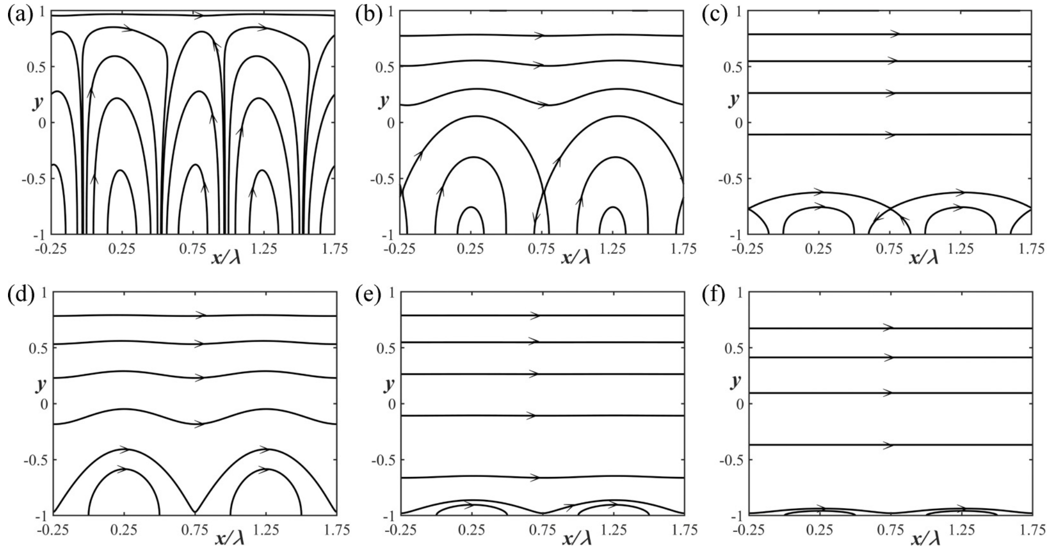

FIG. 4. Flow topologies created by transpiration with $\mathrm{Re}_T = 10$ applied at the lower plate. Figures 4(a)–4(c) $\mathrm{Re} = 10$, $\alpha = 0.1$, 2.0, 10; Figs. 4(d)–4(f) $\mathrm{Re} = 10^3$, $\alpha = 0.1$, 2.0, 10. Thicker lines identify streamlines separating fluid pulled by the upper plate from the fluid injected through the lower plate.

site to the extraction site increases significantly. Theoretical analysis of the limit $\alpha \to 0$ (details not given due to their length) demonstrates that F_1 approaches a finite, α-independent limit proportional to Re and Re_L^2. The same figure demonstrates the reduction of resistance for large α's indicating the dominance of the effects associated with the reduction of the direct contact between the pulled fluid and the plate. The analysis presented in the Appendix shows that this effect is proportional to α^{-3} and is a result of the nonlinear interactions between the first three (0+1+2) modes. The character of variation of F_1 in this limit is well illustrated in Fig. 2(b) which uses the log-log scale for the display of the same data as shown in Fig. 2(a).

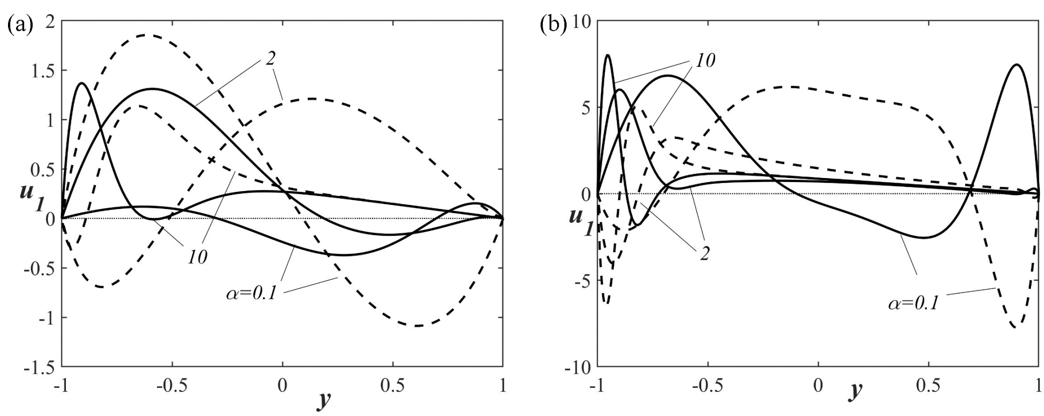

FIG. 5. Distributions of u_1 at locations corresponding to maximum blowing (solid lines) and maximum suction (dashed lines) for $\mathrm{Re} = 10$ [Fig. 5(a)] and $\mathrm{Re} = 10^3$ [Fig. 5(b)]. In Fig. 5(a), data for $\alpha = 2$ is multiplied by 2 and data for $\alpha = 10$ is multiplied by 30 for display purposes. In Fig. 5(b), data for $\alpha = 2$ is multiplied by 5 and data for $\alpha = 10$ is multiplied by 10 for display purposes.

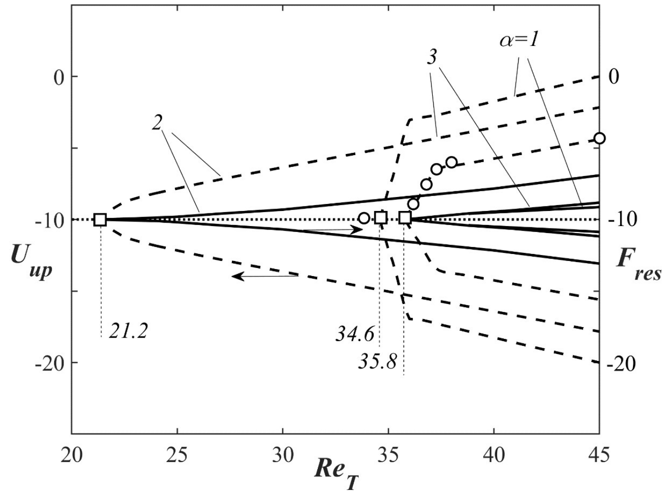

FIG. 6. Variations of the upper plate velocity U_{up} (dashed lines) and the upper plate resistance force F_{res} (solid lines) as functions of Re_T. U_{up} is the upper plate velocity driven by the nonlinear streaming. F_{res} is the resistance force preventing movement of the upper plate exposed to nonlinear streaming. Flow topologies for conditions identified using circles are displayed in Fig. 8.

The above discussion demonstrates that there are always two mechanisms at work, with one dominating for small α's and another dominating for large α's. It turns out that there is the third mechanism, nonlinear streaming, which comes into play for the intermediate α's.

B. Nonlinear streaming

A sufficiently strong transpiration activates a nonlinear streaming effect which propels the fluid and, thus, reduces the magnitude of the external force required to maintain plate movement. To demonstrate this effect, we remove the external force acting at the upper plate and determine if this plate can be propelled solely by transpiration. Assuming that the upper plate does not experience any external resistance, the shear force will accelerate this plate until it reaches a velocity U_{up} which eliminates shear. The required conditions are determined by setting $\mathrm{Re} = 0$ and replacing the boundary condition $u_1^{(0)}(1)$ with $Du_1^{(0)}(1) = 0$. Variations of U_{up} as a function of Re_T displayed in Fig. 6 demonstrate that the plate does not move if Re_T is below a certain critical value $Re_{T,cr}$. Once the critical value is exceeded, the plate starts moving with variations of $U_{\mathrm{up}}(\mathrm{Re}_T)$ following a typical pitchfork bifurcation. The direction of this movement is dictated by edge effects which may be difficult to control. The maximum strength of this effect corresponds to the minimum of $\mathrm{Re}_{T,\mathrm{cr}}$ ($\approx$19.61) which occurs for $\alpha_{\max} = 1.717$ as illustrated in Fig. 7. The strength rapidly diminishes as α moves away from its critical value. The minimum critical $\mathrm{Re}_{T,\mathrm{cr}}$ correlates well with the maximum reduction of resistance (see Fig. 2), which supports the conclusion that the nonlinear streaming contributes to the resistance reduction.

Bifurcation curves demonstrate a rapid increase of U_{up} once Re_T increases above $\mathrm{Re}_{T,\mathrm{cr}}$ followed by a slowdown producing characteristic "corners" on the bifurcation curves (see Fig. 6). These "corners" are more pronounced for α's away from $\alpha_{\max}$ and their formation can be explained by following the evolution of flow patterns along the bifurcation curves. The results presented in Fig. 8 demonstrate that there is a very rapid change in the flow pattern from the symmetric "rolls" below the bifurcation point to a two-layer system consisting of the bottom layer with transpiration "bubbles" and the upper layer with fluid driven along the slot immediately above the bifurcation point. This transition is completed when Re_T increases by about 3–4 above $\mathrm{Re}_{T,\mathrm{cr}}$ and further

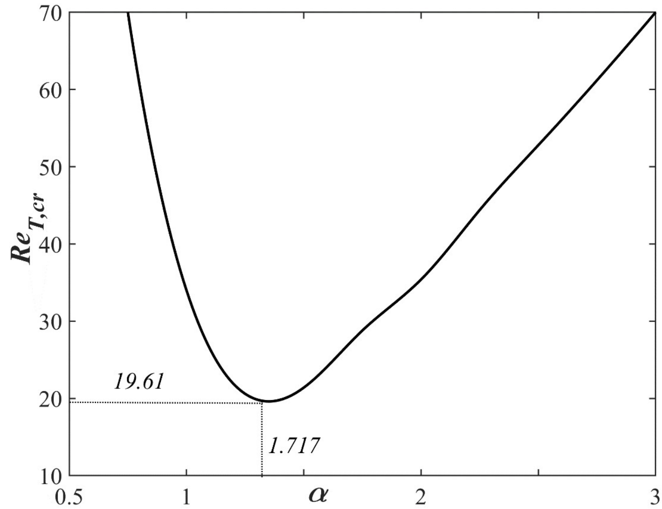

FIG. 7. Variations of the critical value of $\mathrm{Re}_{T,\mathrm{cr}}$ as a function of the transpiration wave number α.

increase of Re_T results in a linear increase of U_{up}, but at a much slower rate when compared to the rate of change immediately past the bifurcation point.

It is of interest to determine the magnitude of the resisting force which would have to be applied to prevent the streaming-driven plate movement. This force is determined by setting $\mathrm{Re} = 0$, returning back to the boundary condition $u_1^{(0)}(1) = 0$, starting with the velocity field corresponding to the right end of the bifurcation curve and slowly reducing Re_T and evaluating the resistance force F_{res}. Variations of F_{res} follow a different pitchfork bifurcation displayed in Fig. 6 and this force disappears below $\mathrm{Re}_{T,\mathrm{cr}}$.

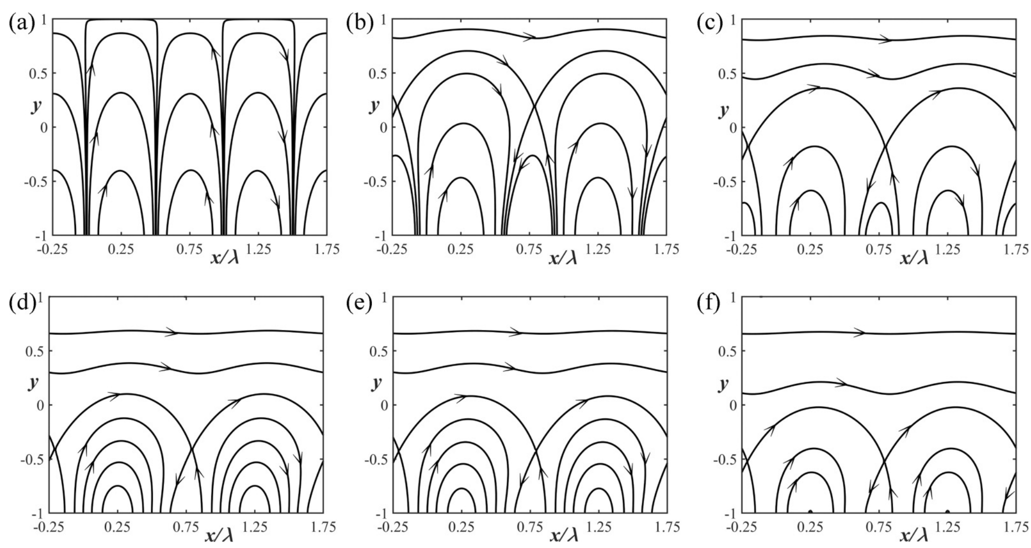

FIG. 8. Topologies of the flow field resulting from the transpiration-induced movement of the upper plate for $\alpha = 3$ and $\mathrm{Re}_T = 34,\ 36,\ 36.5,\ 37,\ 38,\ 45$ in Figs. 8(a), 8(b), 8(c), 8(d), 8(e), and 8(f), respectively.

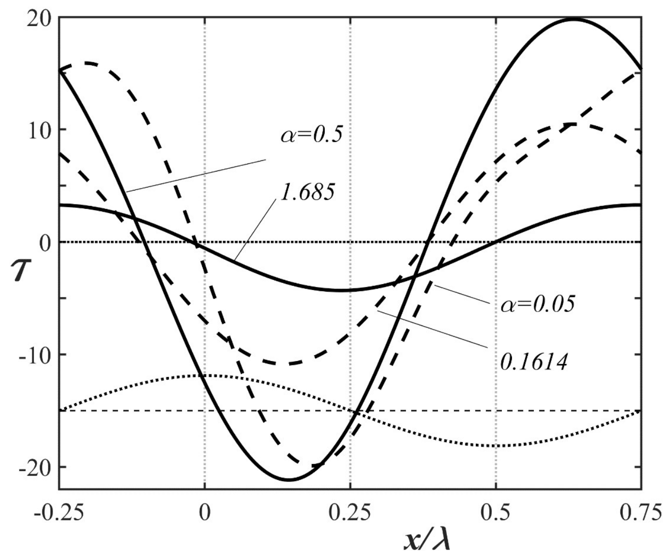

FIG. 9. Distributions of the additional shear $\tau_{\mathrm{ad},U}$ acting on the upper plate for $\mathrm{Re}_T = 10$, $\mathrm{Re} = 10$ (solid line) and $\mathrm{Re} = 10^3$ (dashed lines). The smaller α for each Re corresponds to an increase of resistance while the larger α gives the maximum reduction of resistance. The mean stresses at the upper plate for $\mathrm{Re} = 10$ and $\alpha = (0.5,\ 1.685)$ are $\tau_{U,m} = (1.601, -0.3909)$ and for $\mathrm{Re} = 10^3$ and $\alpha = (0.05,\ 1.614)$ are $\tau_{U,m} = (1.211, -0.3977)$.

C. Description of flow properties

We shall now look at the details of the shear stresses responsible for the movement resistance. The plate shear consists of two components, the original unmodified shear and the transpiration-induced modifications $\tau_{\mathrm{ad},U}$, i.e.,

$$\tau_c(x, 1) = -\frac{1}{2}\mathrm{Re} + \left.\frac{\partial u_1}{\partial y}\right|_{y=1} = -\frac{1}{2}\mathrm{Re} + \tau_{\mathrm{ad},U}. \tag{4.3}$$

The distributions of $\tau_{\mathrm{ad},U}$ illustrated in Fig. 9 are characterized by very large amplitudes (compare with the reference shear of $\frac{1}{2}\mathrm{Re}$ in the unmodified flow) as well as changes of direction. The wave numbers used in this figure correspond to the maximum resistance reduction. The increase of friction occurs approximately in the zone $x \in (0, \frac{\lambda}{2})$, i.e., the zone of the largest reduction of the effective spacing between the plates (see Fig. 3), while a decrease occurs for $x \in (\frac{\lambda}{2},\ \lambda)$ where the spacing reduction is much smaller (but not zero). The velocity distributions displayed in Fig. 10 demonstrate flow acceleration in the zone with the largest reduction of spacing and deceleration in the zone of the smallest reduction. When α is large enough, the decrease of shear dominates resulting in the overall reduction of resistance. Flow topologies displayed in Fig. 3 demonstrate stream displacement away from the lower plate; the effective plate spacing decreases but the transpiration-induced stream "cushioning" near the plate results in the overall decrease of the resistance as the stream "slides" on the "cushion" made of the injected fluid.

Results displayed in Fig. 2 demonstrate the existence of two ranges of transpiration wave numbers; wave numbers smaller than α_{cutoff} lead to an increase of resistance while larger wave numbers lead to a decrease of resistance. Figure 11 demonstrates that α_{cutoff} remains nearly constant for small Re's ($\alpha_{\mathrm{cutoff}} \to 0.728$ for $\mathrm{Re} \to 0$) but rapidly decreases when Re increases above $\sim$10 with this decrease becoming proportional to Re^{-1} for $\mathrm{Re} > \sim$200. Results displayed in Fig. 2 also demonstrate the existence of the most effective wave number $\alpha_{\max}$ leading to the largest reduction of resistance. Variations of $\alpha_{\max}$ as a function of Re displayed in Fig. 11 demonstrate that $\alpha_{\max}$ remains

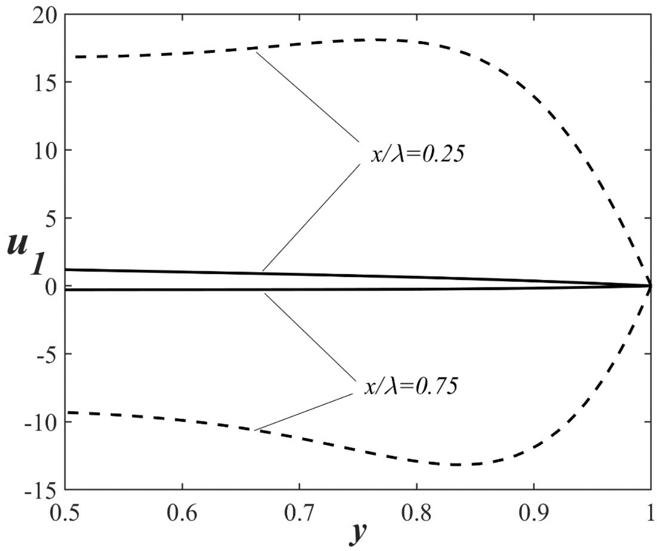

FIG. 10. Distributions of $u_1(y)$ for $\mathrm{Re}_T = 10$, $\mathrm{Re} = 10$ (solid lines, $\alpha = 1.685$) and $\mathrm{Re} = 10^3$ (dashed lines, $\alpha = 0.1614$). The selected α's correspond to the maximum reduction of resistance.

nearly constant for small Re's ($\alpha_{\max} \to 1.816$ for $\mathrm{Re} \to 0$) but rapidly decreases when Re increases above $\sim$10 with this decrease becoming proportional to Re^{-1} for $\mathrm{Re} > \sim$500.

Results displayed in Fig. 12(a) demonstrate that the reduction of the pulling force increases proportionally to Re, reaches a maximum at $\mathrm{Re} \sim 10$ and then starts decreasing proportionally to $\mathrm{Re}^{-1/4}$. It increases proportionally to Re_T^2 within the range of Re_T's of interest as demonstrated in Fig. 12(b). Once Re_T reaches a certain critical value, the reduction of the resistance is equal to the pulling force required to maintain the unmodified flow, i.e., there is no need to use any external force

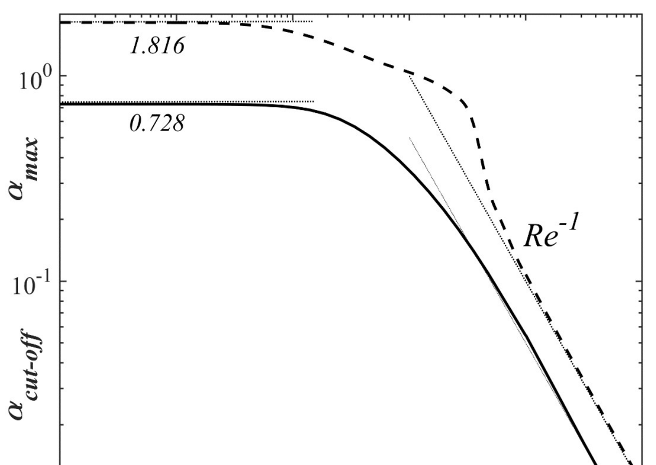

FIG. 11. Variations of the cutoff wave number α_{cutoff} resulting in $F_1 = 0$ (solid line) and the wave number $\alpha_{\max}$ giving the largest reduction of resistance (dashed line) as functions of Re for $\mathrm{Re}_T = 2$.

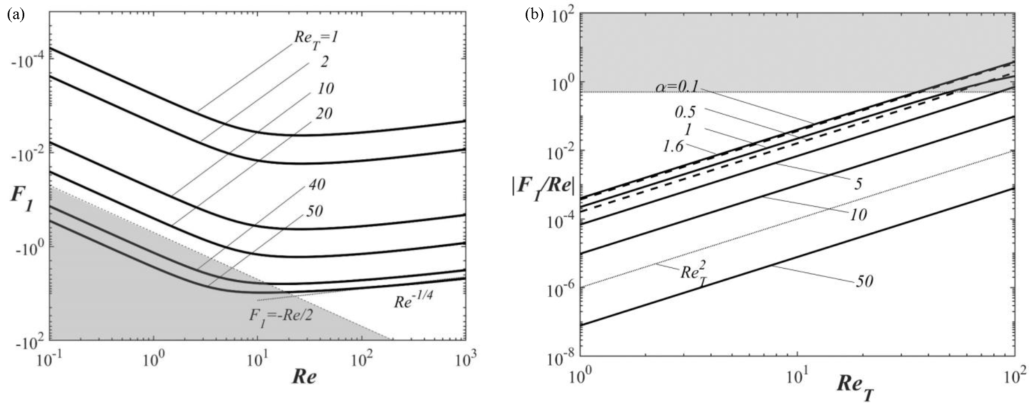

FIG. 12. Variations of the resistance reduction F_1 as a function of Re for $\alpha = 2$ [Fig. 12(a)] and as a function of Re_T [Fig. 12(b)] for $\mathrm{Re} = 10$. Gray areas identify conditions where the transpiration can drive the plate movement without assistance from an external force. Solid (dashed) lines correspond to negative (positive) values.

to maintain the plate movement. When Re_T exceeds this value, an opposite force must be used to prevent plate acceleration. The self-movement on the upper plate can be attributed to the nonlinear streaming effect. Results displayed in Fig. 13 provide an explicit relation between the reduction of the pulling force and the typical flow and transpiration conditions.

D. Energetics

The use of transpiration requires expenditure of additional energy but, at the same time, some energy is saved due to reduction of flow resistance. The net energy cost can be determined by expressing the field equations in terms of the complete flow quantities u_c, v_c, p_c, multiplying the x-momentum equation by u_c, the y-momentum equation by v_c, adding them together and integrating over a control volume extending between the plates in the y direction and over one wavelength in

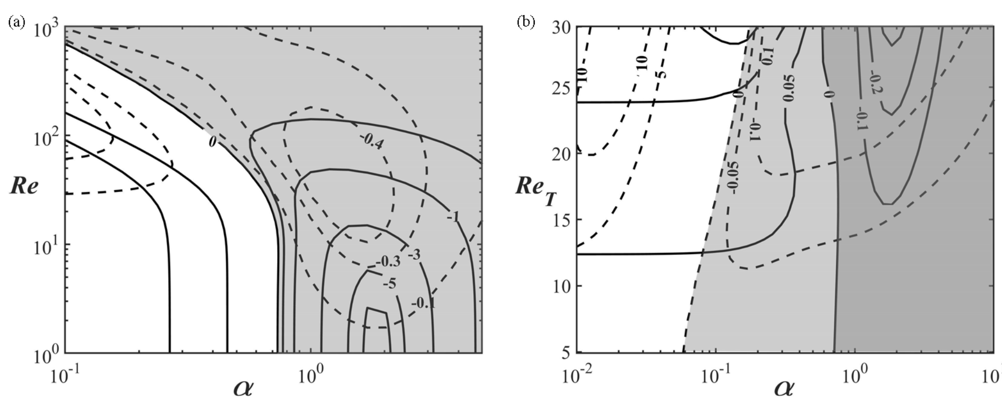

FIG. 13. Variations of the resistance reduction $F_1/(\mathrm{Re} * \mathrm{Re}_T^2)$ (solid lines) and F_1/Re_T^2 (dashed lines) as functions of α and Re for $\mathrm{Re}_T = 10$ are displayed in Fig. 13(a). Variations of F_1/Re for $\mathrm{Re} = 10$ (solid lines) and $F_1/\mathrm{Re} * 100$ for $\mathrm{Re} = 10^3$ (dashed lines) as functions of α and Re_T for are displayed in Fig. 13(b). Gray colors identify conditions leading to the reduction of resistance.

the x direction [26]. The resulting expression has the form

$$\int_0^{\lambda}\int_{-1}^{1}\left(u_c^2\frac{\partial u_c}{\partial x}+u_c v_c\frac{\partial u_c}{\partial y}+u_c v_c\frac{\partial v_c}{\partial x}+v_c^2\frac{\partial v_c}{\partial x}\right)dydx$$
$$=-\int_0^{\lambda}\int_{-1}^{1}\left(u_c\frac{\partial p_c}{\partial x}+v_c\frac{\partial p_c}{\partial y}\right)dydx+\int_0^{\lambda}\int_{-1}^{1}\left(u_c\frac{\partial^2 u_c}{\partial x^2}+u_c\frac{\partial^2 u_c}{\partial y^2}+v_c\frac{\partial^2 v_c}{\partial x^2}+v_c\frac{\partial^2 v_c}{\partial y^2}\right)dydx. \tag{4.4}$$

Rearrange the left-hand side (LHS), integrate by parts, use the continuity equation and periodicity properties to arrive at

$$\text{LHS}=-\frac{1}{2}\int_0^{\lambda}v_c^3\big|_{y=-1}dx \tag{4.5}$$

which represents kinetic energy injected into the flow at the transpiration slots. A similar process applied to the second term on the right-hand side (RHS2) leads to

$$\text{RHS2}=-\int_0^{\lambda}\int_{-1}^{1}\left[\left(\frac{\partial u_c}{\partial x}\right)^2+\left(\frac{\partial u_c}{\partial y}\right)^2+\left(\frac{\partial v_c}{\partial x}\right)^2+\left(\frac{\partial v_c}{\partial y}\right)^2\right]dydx+\int_0^{\lambda}\frac{\partial u_c}{\partial x}\bigg|_{y=1}dx$$
$$=-\text{DIS}(u_c,v_c)+F_{\text{mod}}, \tag{4.6}$$

where $\text{DIS}(u_c, v_c)$ stands for the dissipation function for the modified flow and F_{mod} represents power expenditure associated with the pulling force required to maintain plate movement. The same process applied to the first term on the right-hand side (RHS1) leads to

$$\text{RHS1}=\int_0^{\lambda}(v_c p_c)_{y=-1}dx, \tag{4.7}$$

which represents the work associated with transpiration done at the slots. Use of Eqs. (4.5)–(4.7) in Eq. (4.4) leads to

$$F_{\text{mod}}=-\int_0^{\lambda}\left\{\left[v_c\left(\frac{1}{2}v_c^2+p_c\right)\right]_{y=-1}\right\}dx+\ \text{DIS}(u_c,v_c). \tag{4.8}$$

Use of Eq. (2.2) in Eq. (4.8) results in

$$F_{\text{mod}}=-\int_0^{\lambda}\left\{\left[v_1\left(\frac{1}{2}v_1^2+p_1\right)\right]_{y=-1}\right\}dx+\ \text{DIS}(u_1,v_1)+\frac{1}{2}\lambda\,\text{Re}^2. \tag{4.9}$$

Relation Eq. (4.9) applied to the unmodified flow gives the power required by the unmodified flow as

$$F_{\text{unmod}}=\frac{1}{2}\lambda\,\text{Re}^2. \tag{4.10}$$

The difference between the modified and unmodified powers per unit slot length can be expressed as

$$(F_{\text{mod}}-F_{\text{unmod}})\lambda^{-1}=F_1=-\lambda^{-1}\int_0^{\lambda}\left[v_1\left(\frac{1}{2}v_1^2+p_1\right)\right]_{y=-1}dx+\lambda^{-1}\,\text{DIS}(u_1,v_1) \tag{4.11}$$

and shows that the additional dissipated energy comes either from the work done maintaining the movement of the upper plate or from the work done at the boundaries $\wp=\int_0^{\lambda}[v_1(\frac{1}{2}v_1^2+p_1)]_{y=-1}dx$. When the pulling force is reduced ($F_1<0$), the magnitude of $\wp$ must increase.

We shall now specialize the above relation to the unimodal transpiration described by Eq. (4.1). Use of Eqs. (2.2) and (3.2) in Eq. (4.11) followed by integration result in

$$F_1+\tfrac{1}{4}\,\text{Re}_T\left(p_1^{(1)}+p_1^{(-1)}\right)\big|_{y=-1}=\lambda^{-1}\text{DIS}(u_1,v_1). \tag{4.12}$$

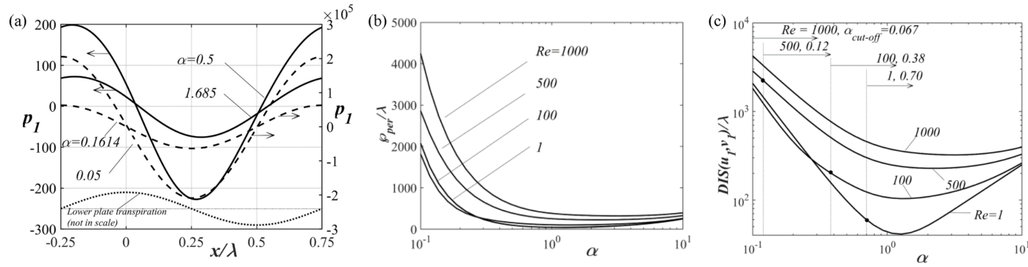

FIG. 14. Distributions of pressure p_1 at the lower plate for Re $= 10$ (solid lines) and Re $= 1000$ (dashed lines) [Fig. 14(a)]. Variations of the work done at the slots $\lambda^{-1}\wp$ as a function of α [Fig. 14(b)]. Variations of the dissipation increase $\lambda^{-1}\mathrm{DIS}(u_1, v_1)$ (see text for details) as a function of α [Fig. 14(c)]. Arrows point in the direction of resistance reduction. All results are for $\mathrm{Re}_T = 10$.

Typical distributions of $p_1(x, -1)$ illustrated in Fig. 14(a) demonstrate a strong dependence on Re. Variations of the rate of work $\lambda^{-1}\wp$ done at the transpiration slots (the second term on the LHS) as a function of α illustrated in Fig. 11(b) show that the minimum of this work occurs for α's where the nonlinear streaming is the most effective. The most energetically effective configuration from the point of view of the reduction of resistance corresponds to the minimization of dissipation $\mathrm{DIS}(u_1, v_1)$ while maintaining $F_1 < 0$. Variations of $\lambda^{-1}\mathrm{DIS}(u_1, v_1)$ with α illustrated in Fig. 11(c) demonstrate that α's to the right of α_{cutoff} provide the largest reduction of resistance at the lowest energy cost.

V. MULTIMODAL TRANSPIRATION AND COMMENSURABILITY EFFECTS

In general, transpiration may have an arbitrary but Fourier-transformable distribution. The analysis so far was focused on distributions characterized but a single Fourier mode, i.e., unimodal transpiration. We shall now asses the effects of more complex distributions by looking at distributions characterized by two wavelenghts λ_β and λ_γ where β and γ are the correspnding wave numbers. The plate-normal velocity distribution at the lower plate has the form

$$v_1(x, -1) = \mathrm{Re}_T V_T [V_\beta \cos(\beta x) + V_\gamma \cos(\gamma x + \Omega)], \tag{5.1}$$

where V_β and V_γ denote the amplitudes of each mode, Ω is the phase difference between them, and V_T is a factor selected to make the difference between the maximum and the minimum of the square bracket unity in view of the scaling described in Sec. II, i.e.,

$$V_T = 1/\max[V_\beta \cos(\beta x) + V_\gamma \cos(\gamma x + \Omega)] - \min[V_\beta \cos(\beta x) + V_\gamma \cos(\gamma x + \Omega)]. \tag{5.2}$$

To investigate the effects of spatial dstributions rather than the effect of the amplitudes of different modes, we take $V_\beta = V_\gamma = 1$ leading to

$$v_1(x, -1) = \mathrm{Re}_T V_T [\cos(\beta x) + \cos(\gamma x + \Omega)]. \tag{5.3}$$

We define the commensurability index as

$$\mathrm{CI} = \frac{\lambda_\beta}{\lambda_\gamma}, \tag{5.4}$$

with CI $= 1$ corresponding to the reference state where both modes have the same wavelengths and their superposition reduces to the case discussed in the previous section with $V_T = \frac{1}{2}$ [see Eq. (5.1)]. In general, the flow system may be either periodic with periodicity defined by CI (commensurable systems) or aperiodic when CI is irrational (noncommensurable systems). The analysis relies on numerical solutions utilizing finite-length computer words which precludes access to noncommensurable distributions. One can nevertheless assess the effects of commensurability by carrying out a

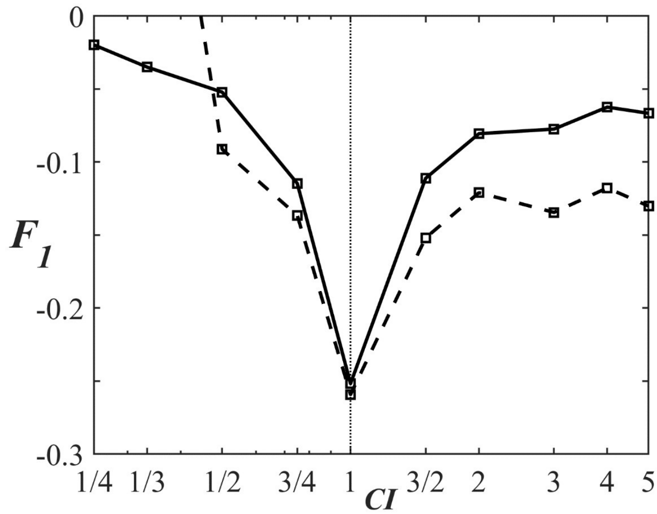

FIG. 15. Variations of the resistance reduction F_1 as a function of the commensurability index CI for $\beta = 1.635$, $\mathrm{Re}_T = 2$, $\mathrm{Re} = 10$ (solid lines) and $\beta = 0.108$, $\mathrm{Re} = 10^3$ (dashed lines). The base wave numbers correspond to the largest resistance reduction.

series of computations for different values of CI. If we assume that the wavelength λ_s of the system is $\lambda_s = m\lambda_\beta = n\lambda_\gamma$, then V_T is a function of Ω which varies in the range $0 \leqslant \Omega \leqslant 2n\pi$.

Figure 15 illustrates typical results obtained for $\beta = 2$ with γ being adjusted to provide the desired value of CI. Only the minimum of F_1 in the whole range of Ω is reported. The results clearly demonstrate that the largest effect is achieved when transpiration is concentrated in a single Fourier mode. Distribution of the transpiration mass flux among different modes rather than concentrating it in a single mode results in a less effective system; CI < 1 gives preference to the long wavelength modulations which increase the resistance while CI > 1 gives preference to the short-wavelength modulations which reduce the resistance reducing potential.

VI. FINITE-SIZE SUCTION/BLOWING SLOTS

Practical application of transpiration for resistance reduction requires the use of finite-size suction/blowing slots in various configurations. One possible arrangement is sketched in Fig. 16(a), where all slots have the same width. Velocity profiles at the outlets/inlets have a parabolic form as the relevant Reynolds number is expected to be small and their maxima are ½ to conform with the scaling introduced in Sec. II. The distribution of the plate normal velocity resulting from transpiration is represented as a Fourier expansion with coefficients determined numerically using fast Fourier transforms. The results displayed in Fig. 16(b) demonstrate a rapid convergence of the computed value of F_1 as the number of Fourier modes N_L used to represent the plate-normal velocity increases. Two Fourier modes are sufficient to represent velocity for large Re's while up to six modes are required for small Re's. These results demonstrate the existence of a reduced distribution model as details of the plate-normal velocity distribution captured by higher Fourier modes are irrelevant as far as the prediction of resistance is concerned.

One is interested in the determination of the slot configuration which produces the smallest F_1. This problem can be solved as a nonlinear constrained optimization problem using the interior point optimization algorithm [32,33]. Since such an optimization method can be trapped in a local minimum [34–36], this problem was solved both as an optimization problem and directly for all

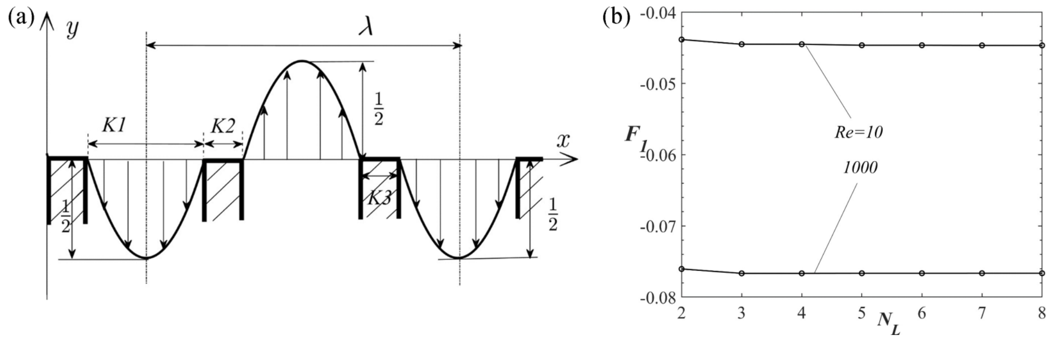

FIG. 16. Sketch of a transpiration system with finite-size slots is displayed in Fig. 16(a). Figure 16(b) illustrates variations of F_1 as a function of the number of Fourier modes N_L used to represent the plate-normal velocity illustrated in Fig. 16(a) for $\mathrm{Re} = 10,\ 10^3$, $\alpha = 2$, $\mathrm{Re}_T = 10$, $K2 = K3 = 0.1\lambda$.

possible parameter combinations. The results displayed in Fig. 17 demonstrate the existence of only global minima under the conditions used in these tests. They demonstrate that F_1 varies widely with variations of the slot geometry with the best performance achieved when the distance between the slots is smallest with the character of variations being similar for a wide range of Re's. A very reasonable estimate of the best performance of such system can be achieved by working with a continuous transpiration described by a single Fourier mode with the wave number dictated by the wavelength of the slot system and the amplitude dictated by the transpiration Reynolds number. This technique can be easily adapted to more complex slot distributions.

Figure 18 illustrates the formation of the nonlinear streaming. Slotted transpiration is less effective in its formation in the sense that the required $\mathrm{Re}_{T,\mathrm{cr}}$ is larger than in the sinusoidal transpiration and the resulting plate velocity is generally smaller. The re-arrangement of the flow topology is much more rapid once the critical conditions are exceeded as illustrated by rapid increase of U_{up} with Re_T immediately past $\mathrm{Re}_{T,\mathrm{cr}}$. These variations become linear once Re_T increases by about 5 beyond its critical value and this is very similar to what was observed for the sinusoidal transpiration (see Fig. 6). These changes occur because "jets" emanating from/entering the slots are more concentrated and thus respond differently to transverse deflections.

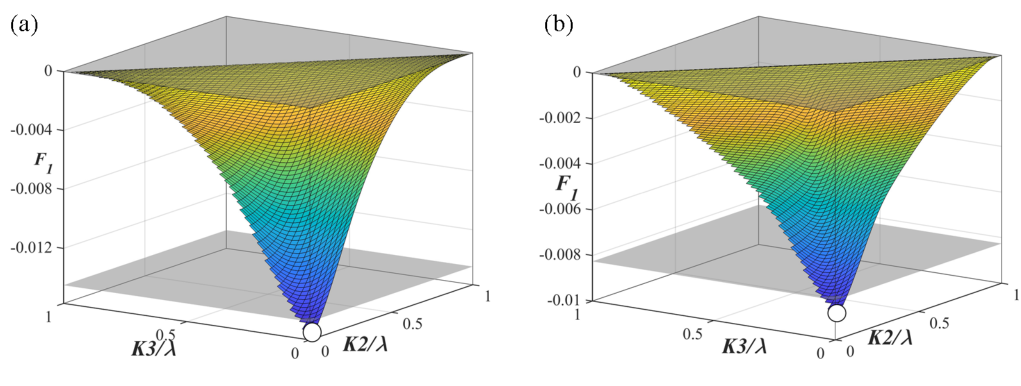

FIG. 17. Variations of change F_1 in the pulling force for the slotted transpiration system sketched in Fig. 16 as a function of the geometric parameters K_2 and K_3 (see Fig. 16 for definitions) for $\mathrm{Re}_T = 2$, $\alpha = 2$, and $\mathrm{Re} = 10$ [Fig. 17(a)] and $\mathrm{Re} = 10^3$ [Fig. 17(b)]. Circles identify the global minima. Grey planes identify F_1 for the sinusoidal transpiration with the same parameters as well as planes for $F_1 = 0$.

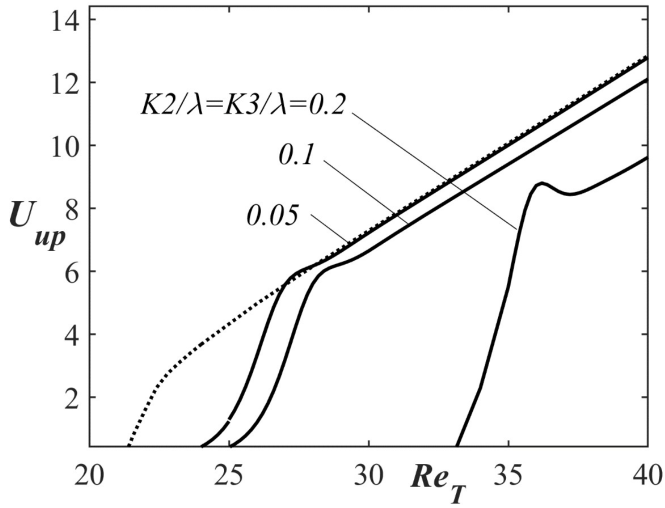

FIG. 18. Variations of the upper plate velocity U_{up} driven by the nonlinear streaming as a function of Re_T for the slotted transpiration with $\alpha = 2$. The dotted line illustrates effects of unimodal transpiration for the same flow parameters.

VII. TRANSPIRATION APPLIED AT THE MOVING PLATE

The analysis carried out so far considered transpiration applied at the stationary plate. When transpiration is applied at the moving plate, the injected/extracted fluid affects the x momentum, which may lead to a different flow response. We have carried out an explicit analysis of such a system to determine its response.

A. Problem formulation and solution method

Since the transpiration system translates with the plate, the proper boundary conditions are of the form

$$u_c(x, -1) = -1, \quad v_c(x, -1) = 0, \tag{7.1a}$$

$$u_c(x, +1) = 0, \quad v_c(x, +1) = \mathrm{Re}_T \sum_{n=-N_L, n\neq 0}^{n=+N_L} s_{T,u}^{(n)} e^{in\alpha(x-t)}, \tag{7.1b}$$

which leads to a time dependent problem which can be converted into a steady problem in a frame of reference moving with the plate using the Galilean transformation of the form

$$X = x - c\,\mathrm{Re}\,t, \quad Y = y, \tag{7.2}$$

where c is the velocity of the moving frame scaled with U_{top} and t is the time scaled with h/U_v; $c = 1$ in view of the scaling used. The field equations and the boundary conditions in the moving frame take the following form:

$$\frac{\partial u_c}{\partial X} + \frac{\partial v_c}{\partial Y} = 0, \tag{7.3a}$$

$$(u_c - \mathrm{Re})\frac{\partial u_c}{\partial X} + v_c\frac{\partial u_c}{\partial Y} = -\frac{\partial p_c}{\partial X} + \nabla^2 u_c, \tag{7.3b}$$

$$(u_c - \mathrm{Re})\frac{\partial v_c}{\partial X} + v_c\frac{\partial v_c}{\partial Y} = -\frac{\partial p_c}{\partial Y} + \nabla^2 v_c, \tag{7.3c}$$

$$u_c(X,-1)=0,\ v_c(X,-1)=0, \tag{7.3d}$$

$$u_c(X,+1)=1, \quad v_c(X,+1)=\mathrm{Re}_T\sum_{n=-N_L,n\neq 0}^{n=+N_L} s_{T,u}^{(n)}e^{in\alpha X}$$

$$\text{with} \quad -\frac{1}{2}\leqslant\sum_{n=-N_G}^{n=N_G} s_{T,u}^{(n)}e^{in\alpha x}\leqslant\frac{1}{2}, \tag{7.3e}$$

$$\left.\frac{\partial p_c}{\partial X}\right|_{\text{mean}}=0. \tag{7.3f}$$

Dividing all dependent variables into the reference quantities and modifications [see Eq. (2.2)] leads to

$$\frac{\partial u_1}{\partial X}+\frac{\partial v_1}{\partial Y}=0, \tag{7.4a}$$

$$(\mathrm{Re}\ u_0+u_1-\mathrm{Re})\frac{\partial u_1}{\partial X}+\mathrm{Re}\ v_1\frac{du_0}{dY}+v_1\frac{\partial u_1}{\partial Y}=-\frac{\partial p_1}{\partial X}+\nabla^2 u_1, \tag{7.4b}$$

$$(\mathrm{Re}\ u_0+u_1-\mathrm{Re})\frac{\partial v_1}{\partial X}+v_1\frac{\partial v_1}{\partial Y}=-\frac{\partial p_1}{\partial Y}+\nabla^2 v_1, \tag{7.4.c}$$

$$u_1(X,-1)=0, \quad v_1(X,-1)=0, \tag{7.4d}$$

$$u_1(X,+1)=0,\ v_1(X,+1)=\mathrm{Re}_T\sum_{n=-N_L,n\neq 0}^{n=+N_L} s_{T,u}^{(n)}e^{in\alpha X}, \tag{7.4e}$$

$$\left.\frac{\partial p_1}{\partial X}\right|_{\text{mean}}=0, \tag{7.4f}$$

where $u_0=\frac{1}{2}(1+Y)$. Introduce the function Ψ defined as $u_1=\partial\Psi/\partial Y$, $v_1=-\partial\Psi/\partial X$ to satisfy the continuity equation. Introduce this function into the X- and Y-momentum equations and eliminate pressure to arrive at

$$\nabla^4\Psi-\mathrm{Re}(u_0-1)\frac{\partial}{\partial X}\nabla^2\Psi+\mathrm{Re}\frac{d^2u_0}{dY^2}\frac{\partial\Psi}{\partial X}=NN(X,Y), \tag{7.5a}$$

$$y=+1:\ \frac{\partial\Psi}{\partial Y}=0, \tag{7.5b}$$

$$\frac{\partial\Psi}{\partial X}=-\mathrm{Re}_T\sum_{n=-N_L,n\neq 0}^{n=+N_L} s_{T,u}^{(n)}e^{in\alpha X}, \tag{7.5c}$$

$$y=-1:\ \frac{\partial\Psi}{\partial Y}=0, \tag{7.5d}$$

$$\frac{\partial\Psi}{\partial X}=0, \tag{7.5e}$$

where the nonlinear term NN is expressed as

$$NN(X,Y)=\frac{\partial}{\partial Y}\left(\frac{\partial\langle u_1u_1\rangle}{\partial X}+\frac{\partial\langle u_1v_1\rangle}{\partial Y}\right)-\frac{\partial}{\partial X}\left(\frac{\partial\langle u_1v_1\rangle}{\partial X}+\frac{\partial\langle v_1v_1\rangle}{\partial Y}\right). \tag{7.5f}$$

The solution is assumed to be in the form of Fourier expansions, i.e.,

$$[\Psi(X,Y), u_1(X,Y), v_1(X,Y), p_1(X,Y), \langle u_1u_1\rangle, \langle u_1v_1\rangle, \langle v_1v_1\rangle, NN]$$
$$= \sum_{n=-\infty}^{n=+\infty} [\Phi^{(n)}(Y), u_1^{(n)}(Y), v_1^{(n)}(Y), p_1^{(n)}(Y), \langle u_1u_1\rangle^{(n)}(y), \langle u_1v_1\rangle^{(n)}(y), \langle v_1v_1\rangle^{(n)}(y),$$
$$\langle NN\rangle^{(n)}(y)]e^{in\alpha X}, \tag{7.6}$$

where $u_1^{(n)} = D\Phi^{(n)}$, $v_1^{(n)} = -in\alpha\Phi^{(n)}$, $D = d/dY$, and all quantities with index (n) are complex conjugates of quantities with index $(-n)$. Substitution of Eq. (7.6) into Eq. (7.6) and separation of Fourier modes lead to modal equations of the form

$$D_n^2\Phi^{(n)} - in\alpha\,\mathrm{Re}(u_0 - 1)D_n\Phi^{(n)} + in\alpha\,\mathrm{Re}\,D^2u_0\,\Phi^{(n)} = NN^{(n)}, \tag{7.7a}$$

$$\Phi^{(n)}(+1) = i\mathrm{Re}_T s_{T,u}^{(n)}/n\alpha \quad \text{for } 1 \leqslant n \leqslant N_L,$$

$$\Phi^{(n)}(+1) = 0 \quad \text{for } n > N_L, \tag{7.7b}$$

$$\Phi^{(n)}(-1) = 0, \quad D\Phi^{(n)}(-1) = 0, \quad D\Phi^{(n)}(+1) = 0 \quad \text{for } -\infty < n < +\infty, \tag{7.7c}$$

$$D\Phi^{(n)}(-1) = 0, \quad D\Phi^{(n)}(+1) = 0 \quad \text{for } -\infty < n < +\infty, \tag{7.7d}$$

where $D^2 = d^2/dY^2$, $D_n = D^2 - n^2\alpha^2$. The final condition comes from the fixed mean pressure gradient constraint. To get its explicit form, insert Eq. (7.6) into the X-momentum equation and extract the aperiodic term to arrive at

$$D^2\Phi^{(0)}(1) - D^2\Phi^{(0)}(-1) = 0, \tag{7.7f}$$

which is the final boundary condition. The above system is solved in the same manner as described in Sec. III. The change F_1 of the pulling force and the change Q_1 of the flow rate are given by Eqs. (2.6) and (2.7), respectively.

B. Discussion

Direct evaluation of the force and the flow rate confirms that they are the same as in the case of transpiration applied at the lower plate. To determine the energy cost, we carry out the energy analysis in the same manner as described in Sec. IVD. The final expression for change in the power requirements is

$$(F_{\mathrm{mod}} - F_{\mathrm{unmod}})\lambda^{-1} = F_1 = \lambda^{-1}\int_0^{\lambda}\left[v_1\left(\frac{1}{2}v_1^2 + p_1\right)\right]_{y=1} dX + \lambda^{-1}\,\mathrm{DIS}(u_1, v_1), \tag{7.8}$$

where the second term on the RHS has a different sign when compared to Eq. (4.11). Specializing this expression to the unimodal transpiration of the form

$$u_1(X, -1) = 0, \quad v_1(X, +1) = \tfrac{1}{2}\mathrm{Re}_T\cos(\alpha X) \tag{7.9}$$

results in

$$F_1 - \tfrac{1}{4}\,\mathrm{Re}_T\big(p_1^{(1)} + p_1^{(-1)}\big)\big|_{y=+1} = \lambda^{-1}\mathrm{DIS}(u_1, v_1), \tag{7.10}$$

where $\lambda^{-1}\wp = \frac{1}{4}\,\mathrm{Re}_T(p_1^{(1)} + p_1^{(-1)})|_{y=+1}$. Results displayed in Fig. 19 demonstrate that the energy cost does not change when transferring transpiration between the plates as such transfer changes the sign of pressure modifications [Fig. 19(a)].

VIII. SUMMARY

We have carried out an analysis of the forces required to maintain the relative movement of parallel plates. The flow resistance is generated by viscous friction and we investigated the use of wall

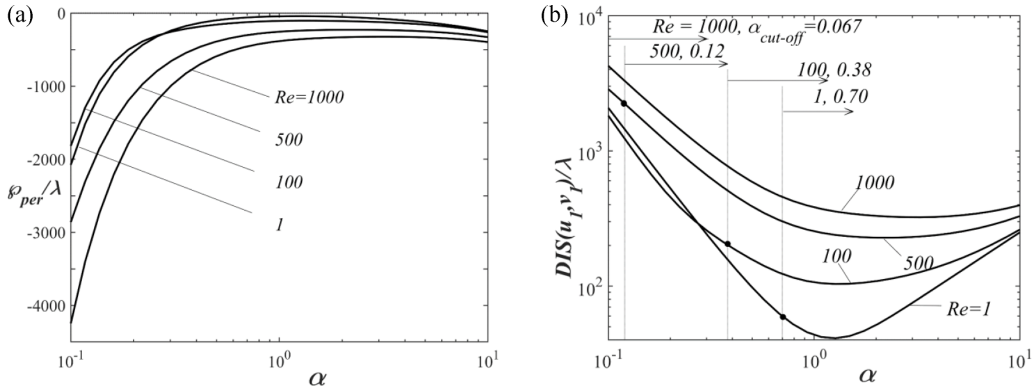

FIG. 19. Variations of the work done at the slots $\lambda^{-1}\wp$ as a function of α [Fig. 19(a)]. Variations of the dissipation increase $\lambda^{-1}\mathrm{DIS}(u_1, v_1)$ (see text for details) as a function of α [Fig. 19(b)]. Arrows point in the direction of resistance reduction. All results are for $\mathrm{Re}_T = 10$.

transpiration for its reduction. The system performance was determined through spectrally accurate numerical solutions of the field equations. We considered arbitrary transpirations made of periodic components. Explicit results are provided only for periodic transpirations as noncommensurable systems are not accessible to computations using finite-length computer words.

It is shown that it is possible to reduce resistance through judicious selection of spatial transpiration patterns. Three effects contributing to these changes have been identified. The first effect is associated with the reduction of the effective spacing between the plates due to formation of a cushion made of transpiration "bubbles" adjacent to the transpired wall leading to an increase of resistance. The second effect is associated with the reduction of the direct contact between the fluid moving along the slot and the transpired plate resulting in a reduction of the wall shear at the transpired plate. The third effect is the nonlinear streaming with produces alternative propulsion and thus contributes to the reduction of the external force required to maintain plate movement. It is shown that the first effect dominates for long-wavelength transpirations resulting in the overall increase of resistance. It is further shown that the second effect dominates for short-wavelength transpirations resulting in the overall reduction of the resistance. It is further shown that the third effect dominates for transpiration wavelengths of O(1) and leads to the largest reduction of the external force required to maintain plate movement. The magnitude of force reduction is proportional to Re_T^2 where the transpiration Reynolds number Re_T measures the transpiration magnitude. It is further shown that transpiration systems have the best performance when transpiration is concentrated in a single transpiration wave number thus avoiding commensurability effects. It is also shown that a good assessment of the performance of real transpiration systems made of finite-size slots can obtained by working with reduced transpiration distribution models and results based on a unimodal transpiration provide a good approximation to the performance of finite-slot-size systems. Analysis of energy requirements associated with the use of transpiration shows that energy savings associated with the reduction of resistance are smaller than the energy cost of transpiration-induced flow changes. In this sense, transpiration is a good candidate for a propulsion augmentation system where part of the propulsion energy is redirected into resistance reduction providing opportunities for the creation of new hybrid propulsion systems. The reduction resistance and the energy costs do not depend on whether the transpiration system is applied at the stationary or at the moving plate.

ACKNOWLEDGMENT

This work has been carried out with the support of China Scholarship Council (201906030152) and NSERC of Canada.

APPENDIX: SHORT-WAVELENGTH ($\alpha \to \infty$) UNIMODAL (SINUSOIDAL) TRANSPIRATION

The amount of fluid inserted/extracted from the slot per half transpiration wavelength decreases proportionally to $1/\alpha$ resulting in small flow modulations (see Fig. 3). Assume that the solution can be represented as power series in terms of a small parameter ε expressing the magnitude of the modulations of the form

$$u_1 = \varepsilon \hat{u}_1 + \varepsilon^2 \hat{u}_2 + 0(\varepsilon^3), \quad v_1 = \varepsilon \hat{v}_1 + \varepsilon^2 \hat{v}_2 + 0(\varepsilon^3), \quad p_1 = \varepsilon \hat{p}_1 + \varepsilon^2 \hat{p}_2 + 0(\varepsilon^3). \tag{A1}$$

Substitute Eq. (A1) into Eqs. (2.3)–(2.5) and extract the leading-order system

$$-\frac{\partial \hat{p}_1}{\partial x} + \frac{\partial^2 \hat{u}_1}{\partial x^2} + \frac{\partial^2 \hat{u}_1}{\partial y^2} - \text{Re}\, u_0 \frac{\partial \hat{u}_1}{\partial x} - \text{Re}\, \frac{du_0}{dy} \hat{v}_1 = 0 \tag{A2}$$

$$-\frac{\partial \hat{p}_1}{\partial y} + \frac{\partial^2 \hat{v}_1}{\partial x^2} + \frac{\partial^2 \hat{v}_1}{\partial y^2} - \text{Re}\, u_0 \frac{\partial \hat{v}_1}{\partial x} = 0, \tag{A3}$$

$$\frac{\partial \hat{u}_1}{\partial x} + \frac{\partial \hat{v}_1}{\partial y} = 0, \tag{A4}$$

$$\hat{u}_1(1) = 0, \quad \hat{u}_1(-1) = 0, \quad \hat{v}_1(1) = 0, \quad \hat{v}_1(-1) = \frac{1}{4}\text{Re}_T (e^{i\alpha x} + e^{-i\alpha x}), \tag{A5}$$

whose solution has the form of

$$[\hat{u}_1, \hat{v}_1, \hat{p}_1](x, y) = [\tilde{u}_1, \tilde{v}_1, \tilde{p}_1](y) e^{i\alpha x} + [\tilde{u}_1^*, \tilde{v}_1^*, \tilde{p}_1^*](y) e^{-i\alpha x}, \tag{A6}$$

where stars denote complex conjugates. Substitution of Eq. (A6) into Eqs. (A2)–(A5) and elimination of $\tilde{u}_1$ and $\tilde{p}_1$ result in a fourth-order boundary value problem of the form

$$[(D^2 - \alpha^2)^2 - i\alpha \text{Re} u_0 (D^2 - \alpha^2) - i\alpha \text{Re} D^2 u_0] \tilde{v}_1 = 0, \tag{A7}$$

$$\tilde{v}_1(-1) = \tfrac{1}{4}\text{Re}_T, \quad D\tilde{v}_1(-1) = 0, \quad \tilde{v}_1(1) = 0, \quad D\tilde{v}_1(1) = 0, \tag{A8}$$

where $D = d/dy$. Equations (A7) and (A8) are solved numerically using Galerkin method combined with Chebyshev expansion for $\tilde{v}_1$. The next order system takes the following form:

$$-\frac{\partial \hat{p}_2}{\partial x} + \frac{\partial^2 \hat{u}_2}{\partial x^2} + \frac{\partial^2 \hat{u}_2}{\partial y^2} - \text{Re}\, u_0 \frac{\partial \hat{u}_2}{\partial x} - \text{Re}\, \frac{du_0}{dy} \hat{v}_2 = \hat{u}_1 \frac{\partial \hat{u}_1}{\partial x} + \hat{v}_1 \frac{\partial \hat{u}_1}{\partial y}, \tag{A9}$$

$$-\frac{\partial \hat{p}_2}{\partial y} + \frac{\partial^2 \hat{v}_2}{\partial x^2} + \frac{\partial^2 \hat{v}_2}{\partial y^2} - \text{Re}\, u_0 \frac{\partial \hat{v}_2}{\partial x} = \hat{u}_1 \frac{\partial \hat{v}_1}{\partial x} + \hat{v}_1 \frac{\partial \hat{v}_1}{\partial y}, \tag{A10}$$

$$\frac{\partial \hat{u}_2}{\partial x} + \frac{\partial \hat{v}_2}{\partial y} = 0, \tag{A11}$$

$$\hat{u}_2(1) = 0, \quad \hat{u}_2(-1) = 0, \quad \hat{v}_2(1) = 0, \quad \hat{v}_2(-1) = 0. \tag{A12}$$

Analysis of Eqs. (A9)–(A12) shows that its solution can be represented as

$$[\hat{u}_2, \hat{v}_2](x, y) = [\tilde{u}_{20}, \tilde{v}_{20}](y) + [\tilde{u}_{22}, \tilde{v}_{22}](y) e^{2i\alpha x} + [\tilde{u}_{22}^*, \tilde{v}_{22}^*](y) e^{-2i\alpha x}, \tag{A13a}$$

$$\hat{p}_2(x, y) = \tilde{p}_{20}(y) + \tilde{p}_{22}(y) e^{2i\alpha x} + \tilde{p}_{22}^*(y) e^{-2i\alpha x}. \tag{A13b}$$

Substitution of Eq. (A13) into Eqs. (A9)–(A12) and extraction of mode zero lead to conclusion that $\tilde{v}_{20} = 0$ and that $\tilde{u}_{20}$ is described by the following boundary value problem:

$$D^2 \tilde{u}_{20} = \tilde{v}_1 D\tilde{u}_1^* + \tilde{v}_1^* D\tilde{u}_1, \quad \tilde{u}_{20}(-1) = 0, \quad \tilde{u}_{20}(1) = 0, \tag{A14}$$

which is solved using Chebyshev expansion combined with Galerkin procedure. Use of Eq. (2.6) leads to

$$F_1 = \varepsilon^2 \lambda^{-1} \int_0^{\lambda} \left. \frac{d\tilde{u}_{20}}{dy} \right|_{y=1} dx = \varepsilon^2 \left. \frac{d\tilde{u}_{20}}{dy} \right|_{y=1}. \tag{A16}$$

If one defines ε as α^{-1}, the above analysis shows that F_1 should be $0(\alpha^{-2})$ for $\alpha \to \infty$. The formation of boundary layer at the stationary plate results in $\frac{d\tilde{u}_{20}}{dy}|_{y=1} = 0(\alpha)$, which leads to $F_1 = 0(\alpha^{-3})$. The above solution also shows that $F_1 = 0(\mathrm{Re}_T^2)$.

---

[1] D. Gropper, L. Wang, and T. J. Harvey, Hydrodynamic lubrication of textured surfaces: A review of modeling techniques and key findings, Tribol. Int. **94**, 509 (2016).
[2] V. A. Romanow, Stability of plane-parallel Couette flow, Funct. Anal. Appl. **7**, 137 (1972).
[3] K. Deguchi and M. Nagata, Bifurcations and instabilities in sliding Couette flow, J. Fluid Mech. **678**, 156 (2011).
[4] J. M. Floryan, Centrifugal instability of Couette flow over a wavy wall, Phys. Fluids **14**, 312 (2002).
[5] H. V. Moradi and J. M. Floryan, Sliding Couette flow in a ribbed annulus, Phys. Fluids **28**, 074103 (2016).
[6] J. M. Floryan, Wall-transpiration-induced instabilities in plane Couette flow, J. Fluid Mech. **488**, 151 (2003).
[7] P. Gittler, Stability of Poiseuille–Couette flow between concentric cylinders, Acta Mech. **101**, 1 (1993).
[8] M. J. Walsh, Riblets as a viscous drag reduction technique, AIAA J. **21**, 485 (1983).
[9] A. Mohammadi and J. M. Floryan, Effects of longitudinal grooves on the Couette-Poiseuille flow, J. Theor. Comput. Fluid Mech. **28**, 549 (2014).
[10] J. M. Floryan, S. Shadman, and M. Z. Hossain, Heating-induced drag reduction in relative movement of parallel plates, Phys. Rev. Fluids **3**, 094101 (2018).
[11] J. M. Floryan, Stability of wall bounded shear layers with simulated distributed surface roughness, J. Fluid Mech. **335**, 29 (1997).
[12] J. Szumbarski and J. M. Floryan, Tollmien-Schlichting instability of channel flow in the presence of weak distributed suction, AIAA J. **38**, 372 (2000).
[13] P. J. D. Roberts, J. M. Floryan, G. Casalis, and D. Arnal, Boundary layers instability induced by wall suction, Phys. Fluids **13**, 2543 (2001).
[14] P. J. D. Roberts and J. M. Floryan, Instability of accelerated boundary layers induced by surface suction, AIAA J. **40**, 851 (2002).
[15] P. J. D. Roberts and J. M. Floryan, Instability of adverse-pressure-gradient boundary layers with suction, AIAA J. **46**, 2416 (2008).
[16] J. M. Floryan, K. Yamamoto, and T. Murase, Laminar-turbulent transition in plane Poiseuille flow in the presence of simulated wall roughness, CASI J. **38**, 173 (1992).
[17] J. Ou, B. Perot, and J. P. Rothstein, Laminar drag reduction in microchannels using ultrahydrophobic surfaces, Phys. Fluids **16**, 4635 (2004).
[18] A. Inasawa, C. Ninomiya, and M. Asai, Suppression of tonal trailing-edge noise from an airfoil using a plasma actuator, AIAA J. **51**, 1695 (2013).
[19] T. Kato, Y. Fukunishi, and R. Kobayashi, Artificial control of the three-dimensionalization process of T-S waves in boundary-layer transition, JSME Int. J. **40**, 536 (1997).
[20] Y. Fukunishi and I. Ebina, Active control of boundary-layer transition using a thin actuator, JSME Int. J. **44**, 24 (2001).
[21] J. M. Floryan and S. Zandi, Reduction of pressure losses and increase of mixing in laminar flows through channels with long-wavelength vibrations, J. Fluid Mech. **864**, 670 (2019).
[22] J. L. Bansal and N. C. Jain, On the plane Couette flow of a viscous compressible fluid with transpiration cooling, Proc. Indian Acad. Sci. **80**, 1 (1974).
[23] K. Singh, Three-dimensional Couette flow with transpiration cooling, Z. angew. Math. Phys. **50**, 661 (1999).
[24] G. Huang, Y. Zhu, Z. Y. Liao, Z. Huang, and P. X. Jiang, Transpiration cooling with bio-inspired structured surfaces, Bioinspir. Biomimet. **15**, 036016 (2020).
[25] T. R. Bewley, A fundamental limit on the balance of power in a transpiration-controlled channel flow, J. Fluid Mech. **632**, 443 (2009).

[26] D. Floryan (private communication).
[27] M. Quadrio, J. M. Floryan, and P. Luchini, Modification of turbulent flow using distributed suction, CASI J. **51**, 61 (2005).
[28] M. Quadrio, J. M. Floryan, and P. Luchini, Effect of streamwise-periodic wall transpiration on turbulent friction drag, J. Fluid Mech. **576**, 425 (2007).
[29] S. Koganezawa, A. Mitsuishi, T. Shimura, K. Iwamoto, H. Mamori, and A. Murata, Pathline analysis of traveling wavy blowing and suction control in turbulent pipe flow for drag reduction, Int. J. Heat Fluid Flow **77**, 388 (2019).
[30] M. Z. Hossain, D. Floryan, and J. M. Floryan, Drag reduction due to spatial thermal modulations, J. Fluid Mech. **713**, 398 (2012).
[31] C. Canuto, M. Y. Hussaini, A. Quarteroni, and T. A. Zang, *Spectral Methods* (Springer, Berlin, 1996).
[32] T. F. Coleman and Y. Li, On the convergence of interior-reflective Newton method for nonlinear minimization subject to bounds, Math. Program. **67**, 189 (1994).
[33] T. F. Coleman and Y. Li, An interior trust region approach for nonlinear minimization subject to bounds, SIAM J. Optimiz. **6**, 418 (1996).
[34] R. H. Byrd, M. E. Hribar, and J. Nocedal, An interior point algorithm for large-scale nonlinear programming, SIAM J. Optimiz. **9**, 877 (1999).
[35] R. H. Byrd, J. C. Gilbert, and J. Nocedal, A trust region method based on interior point techniques for nonlinear programming, Math. Program. Ser. A **89**, 149 (2000).
[36] R. A. Waltz, J. L. Morales, J. Nocedal, and D. Orban, An interior algorithm for nonlinear optimization that combines line search and trust region steps, Math. Program. Ser. A **107**, 391 (2006).